

1 **Models of primate ventral stream that categorize and visualize images**

2 Elijah Christensen¹, Joel Zylberberg^{2,3}

3 ¹Department of Physiology and Biophysics, University of Colorado Anschutz Medical Campus

4 ²Learning in Machines and Brains Program, CIFAR, Toronto, ON Canada

5 ³Centre for Vision Research, and Department of Physics and Astronomy, York University, Toronto, ON

6 Canada

7 **Abstract**

8 **An open question in systems neuroscience is which objective function (or computational “goal”)**

9 **best describes the computations performed by the ventral stream (VS) of primate visual cortex.**

10 **Substantial past research has suggested that object categorization could be such a goal. Recent**

11 **experiments, however, showed that information about object positions, sizes, etc. is encoded with**

12 **increasing explicitness along this pathway. Because that information is not necessarily needed for**

13 **object categorization, this motivated us to ask whether primate VS may do more than “just”**

14 **object recognition. To address that question, we trained deep neural networks, all with the same**

15 **architecture, with three different objectives: a supervised object categorization objective; an**

16 **unsupervised autoencoder objective; and a semi-supervised objective that combined autoencoding**

17 **with categorization. We then compared the image representations learned by these models to**

18 **those observed in areas V4 and IT of macaque monkeys using canonical correlation analysis**

19 **(CCA). We found that the semi-supervised model provided the best match the monkey data,**

20 **followed closely by the unsupervised model, and more distantly by the supervised one. These**

21 **results suggest that multiple objectives – including, critically, unsupervised ones – might be**

22 **essential for explaining the computations performed by primate VS.**

23

Introduction

24 The ventral stream (VS) of visual cortex begins in primary visual cortex (V1), ends in inferior temporal
25 cortex (IT), and is essential for object recognition. Accordingly, a long-standing hypothesis in the field
26 is that the ventral stream could be understood as mapping visual scenes onto neuronal firing patterns that
27 represent object identity¹⁻⁵. Supporting that assertion, deep convolutional neural networks (DCNN's)
28 trained to categorize objects in natural images develop intermediate representations that resemble those
29 in primate VS^{2,6-8}. At the same time, VS and other visual areas are also engaged during visualization of
30 both previously encountered and novel scenes^{9,10}, suggesting that the VS can *generate* visual scenes in
31 addition to identifying objects within those scenes. Furthermore, non-categorical information, about
32 object positions¹¹, sizes, etc. is also represented with increasing explicitness in late VS areas V4 and
33 IT¹². This non-categorical information is not necessarily needed for object recognition tasks, although
34 interestingly, deep convolutional neural networks (CNNs) recapitulated this trend of increasingly
35 explicit category-orthogonal representations with increasing depth¹¹. Nevertheless these recent findings
36 motivated us to reconsider the long-standing question: What computational objective best explains VS
37 physiology¹³⁻¹⁵?

38 To address this question, we pursued a recently-popularized approach^{2,7,8,12,14,15} and trained deep neural
39 networks to perform one of three different tasks, each of which corresponds to a different computational
40 objective. We trained the networks to either: a) recognize objects; b) form compressed image
41 representations that suffice for reconstructing the input image; or c) recognizing objects while *also*
42 retaining enough information about the input image to allow its reconstruction. We then compared these
43 trained neural networks' responses to image stimuli to responses observed in neurophysiology
44 experiments wherein monkeys saw the same images that were input to the models, to see which tasks
45 yielded models that best matched the neural data. We used the same architecture for all of these
46 networks, ensuring that any differences in how well the models recapitulate the neural data can be

47 attributed to their objective function, and not to architecture differences. Our main finding is that
48 networks trained with objective (c) provided the closest match for both areas V4 and IT of the monkey,
49 closely followed by ones trained with objective (b), and more distantly followed by the networks trained
50 on the pure object recognition objective (a). This suggests that a full understanding of visual ventral
51 stream computations might require considerations beyond object recognition, and that scene
52 reconstruction is a promising candidate for the “other” computations occurring within the VS. Notably,
53 other work¹⁴⁻¹⁸, including two concurrent studies^{14,15}, has asked whether unsupervised image processing
54 models can describe primate VS function. We discuss our findings in the context of these concurrent
55 studies in the Discussion.

56 **Results**

57 **Computational Models**

58 To identify the degree to which different computational objectives describe ventral stream physiology,
59 we optimized deep convolutional neural network (CNN) models for different objectives, and compared
60 them to neural recordings from the primate ventral stream. Each computational model was constructed
61 out of a series of layers of artificial neurons, connected sequentially. The first layer takes as input an
62 image x and at the final layer outputs a set of neuronal activities that represent the visual scene input
63 (Fig 1B), including object identity. We refer to this output as the *latent representation*. The input
64 images, x , consisted of images of clothing articles superimposed over natural image backgrounds (see
65 Methods). Each image used a single clothing article rendered in a randomly chosen position and
66 orientation, and placed over a natural image background (Fig. 1A).

67 The models each had a total of four layers of processing between their inputs and these latent
68 representations. The visual inputs to the model had normalized luminance values, mimicking the
69 normalization observed at LGN¹⁹. The connectivity between neurons in each layer (and the artificial

70 neurons' biases) were optimized within each model, to achieve the specified objective (see Methods).

71 We repeated this process for three different objectives, yielding three different types of models. The first

72 type of model was optimized strictly for object recognition: the optimization maximized the ability of a

73 linear decoder to determine the identity of the clothing object in the visual scene from the latent

74 representation. (This mirrors the observation that neural activities in area IT can be linearly decoded to

75 recover object identity¹²). We refer to this network as the “classify” network. The second type of model

76 was optimized for the ability of a decoder network to reconstruct the object from the latent

77 representation. We refer to this autoencoder as the “reconstruct” model. Finally, we considered a model

78 whose objective during training is the sum of the “classify” objective and the “reconstruct” one: the

79 optimization simultaneously maximized this network’s ability to perform both tasks, and we refer to it as

80 the “combined” model. This combined model is a semi-supervised autoencoder, the construction of

81 which was motivated by previous work in machine learning²⁰.

82 In all cases, the models were optimized via backpropagation using sets of images containing randomly

83 sampled objects, until their object classification performance saturated on a set of held-out validation

84 images. Reasonable performance on the categorization task was obtained the “classify” and “combined”

85 models (Fig 1D); as expected, the “reconstruct” model had very poor classification performance.

86 Similarly, we assessed the ability of an optimized generator network to decode the latent state

87 activations to reconstruct the input images. After training, both the “combined” model, and the

88 “reconstruct” model, had relatively low reconstruction errors, whereas the “classify” model, had much

89 higher reconstruction error. Thus, we created neural networks that could either classify image contents

90 but not reconstruct the images themselves (“classify”), reconstruct but not classify (“reconstruct”), or do

91 both tasks with reasonable efficacy (“combined”).

92 Having developed models optimized for these different objectives, we could evaluate how well each
93 model matched observations from primate VS, and use that comparison to determine which
94 computational objective provides the best description of primate VS.

95 **Electrophysiology Comparisons**

96 To compare our neural network models to ventral stream physiology, we used the experimental data
97 from a previously-published study^{12,21} (see Methods and Refs. 12,21 for details). These data consisted of
98 electrode array recordings from areas V4 and IT of monkeys that were viewing images of objects
99 superimposed over natural image backgrounds, at different locations and orientations. Many neurons in
100 each area were simultaneously observed in these experiments.

101 First, we asked how well each layer within each neural network model matched the primate VS data. To
102 achieve this goal, we input into our models the same images that were shown to the monkeys in the
103 physiology experiments. We then extracted the activations of the artificial neurons at each layer of our
104 computational models, and we used Canonical Correlation Analysis (CCA)^{22,23} to compare those
105 artificial neurons' activations to those recorded in monkey V4 and IT (See Methods). In brief, CCA
106 assesses the degree to which weighted sums of our neural network unit activations correlate with
107 weighted sum of the neuron firing rates observed in the monkey experiments. It can thus test for
108 similarity in how the images are represented by the neural networks, and the monkey, without requiring
109 us to assign each neural network unit to a specific neuron in the monkey experiments. Similar to regular
110 correlation analysis, CCA correlations of 0 indicate no relation between the neural network and monkey
111 visual representations, while a value of 1 indicate perfect similarity. We extracted the canonical
112 correlations for the first 10 CCA components, and averaged their values (Fig. 2).

113 For the “classify” model, IT was best described by the latent representation (z), whereas V4 was better
114 described by the conv3 layer, which is earlier in the hierarchy. This in line with previous work (e.g.,

115 Refs. 4,17) showing that deeper layers of task-trained neural networks are better matches to brain
116 regions deeper in the ventral stream’s visual hierarchy. For contrast, with our “reconstruct” and
117 “combined” objectives – which involve an unsupervised component – the best match to both the V4 and
118 the IT data, was from the latent representation (z) of the neural network. This suggests that the specific
119 alignment of which brain area is best matched by which layer of an artificial neural network model
120 could depend on the task for which the artificial neural network is optimized.

121 To determine which objective function led to neural networks that best match each brain area, we
122 identified the layer of each network that gave the highest mean canonical correlation with each brain
123 region. For area IT, this was the latent representation (z) in all models; whereas for area V4, this was the
124 latent representation (z) for the “reconstruct” and “combined” models, and layer conv3 for the “classify”
125 model. We then compared these best-layer mean canonical correlation values between neural network
126 models, for each brain area, to determine which model(s) best described the brain data.

127 For area IT, the “combined” model had the highest mean canonical correlation value (0.265 +/- 0.002:
128 mean +/- standard error, over 15 random samplings of neural network unit activations; see Methods),
129 followed closely by the “reconstruct” model (0.262 +/- 0.003: mean +/- standard error, over 15 random
130 samplings of neural network unit activations), and more distantly by the “classify” model (0.240 +/-
131 0.005: mean +/- standard error, over 15 random samplings of neural network unit activations). The
132 differences between models was statistically significant in all cases ($p = 1 \times 10^{-2}$ for comparing the
133 “combined” and “reconstruct” models; $p = 2 \times 10^{-6}$ for comparing the “combined” and “classify” models;
134 and $p = 2 \times 10^{-6}$ for comparing the “reconstruct” and “classify” models. All comparisons were done with
135 one-tailed Wilcoxon rank sum tests.)

136 Our findings in area V4 mirrored those from IT: the “combined” model had the highest mean canonical
137 correlation value (0.245 +/- 0.004: mean +/- standard error, over 15 random samplings of neural network
138 unit activations), followed closely by the “reconstruct” model (0.239 +/- 0.005: mean +/- standard error,

139 over 15 random samplings of neural network unit activations), and more distantly by the “classify”
140 model (0.21 ± 0.01 : mean \pm standard error, over 15 random samplings of neural network unit
141 activations). The differences between models was statistically significant in all cases ($p = 2 \times 10^{-3}$ for
142 comparing the “combined” and “reconstruct” models; $p = 2 \times 10^{-6}$ for comparing the “combined” and
143 “classify” models; and $p = 2 \times 10^{-6}$ for comparing the “reconstruct” and “classify” models. All
144 comparisons done with one-tailed Wilcoxon rank sum test.)

145 Having identified the best models, and motivated by the analyses by in Ref. 12, we asked how the
146 different attributes in the input images – both categorical and non-categorical -- were represented by the
147 different models. We first tested the position sensitivity of the units in each layer of the neural network
148 model, using test images of clothing items on the natural scene backgrounds (Fig. 3AB; see Methods).
149 For both the “reconstruct” and “combined” models, the position sensitivity increased monotonically
150 with increasing depth. Whereas, for the “classify” model, the position sensitivity decreased between
151 conv4 and the subsequent latent representation (z). (Notably, all layers before the latent representation in
152 our model are convolutional, whereas the latent representation is a *fully connected layer*. For
153 comparison, the authors of Ref. 12 showed position sensitivity in their model – trained purely for
154 categorization – that increased monotonically with depth, for the 6 convolutional layers of their model.
155 This could seem at odds with the fact that our latent representation is less position sensitive than are the
156 previous layers. However, the fully connected nature of this layer will tend to remove position
157 information, and hence we believe that our results are quite consistent with those of Ref. 12. in terms of
158 position information evolving with depth in fully convolutional neural network layers.).

159 For comparison, we show the position selectivity from the neurons observed in the monkey experiments,
160 which show increasing position selectivity between V4 and IT.

161 Next, we tested the rotation selectivity of each of the units in our models. Those were quite low for the
162 units in all of the models, as they were in V4 and IT of the monkey (Fig. 3C). The one exception to this

163 is the latent representation of the “classify” model, which stood out for its high rotation selectivity.

164 Finally, we assessed the category selectivity of the units in each of our models, and show them alongside

165 the corresponding data from monkey V4 and IT (Fig. 3D). Notably, the latent space of the “classify”

166 network stands out for its high category selectivity, compared with the other network models, and the

167 monkey data.

168 Importantly, the monkey data in Fig. 3 were derived from the images shown to the monkeys, whereas

169 we computed the selectivities of our neural network model units on the images of clothing items

170 superimposed on nature image backgrounds. We did this because the image categories in those images

171 (clothing images) match those on which the network models were trained; these are different from the

172 objects in the images shown to the monkeys. This is a potential limitation in the comparisons between

173 network models and monkey data in Fig. 3.

174 Discussion

175 Here, we studied a supervised learning model (trained to classify objects in images), an unsupervised

176 learning model (trained as an autoencoder to generate compressed representations of input images that

177 suffice for their reconstruction), and a semi-supervised model (trained to both classify objects and

178 enable image reconstruction from its latent representation). We asked which objective function led to

179 neural network models whose image representations most closely match those observed in the ventral

180 stream of the primate visual cortex, and found that the best match was the semi-supervised model. The

181 unsupervised model was close behind, while the supervised model lagged more substantially behind the

182 other two. This suggests that accurate descriptions of ventral stream computations should involve

183 unsupervised learning objectives (e.g., image reconstruction). We also characterized the depth-

184 depending evolution of categorical and non-categorical information in these models, with an aim

185 towards understanding how the different objectives affect the representation of different image attributes

186 at different depths in the neural networks.

187

188 We are not the first to explore unsupervised learning algorithms as models of ventral stream (VS)
189 computation. For example, the classic “sparse coding” models showed that unsupervised autoencoders
190 formed image representations similar in many ways to those observed in primary visual cortex
191 (V1)^{18,24,25}. More recent work showed that better descriptions of primate V1 responses could be obtained
192 with supervised learning algorithms trained for object recognition^{16,17} than with the unsupervised
193 algorithms¹⁶, or with wavelet bases that mimic those learned by the unsupervised learning algorithms¹⁷.
194 Those works did not look at deeper areas of the VS (e.g., V4 or IT), nor did they study the different
195 objectives in the same neural network architectures.

196 Two concurrent studies^{14,15} overcome these challenges – as does this paper. Those studies also
197 investigated unsupervised deep learning algorithms, and found that they better matched VS image
198 representations than do supervised algorithms. This is at odds with earlier studies (e.g. Refs. 2,4), which
199 suggested that supervised algorithms (like our “classify” model) would be the best, although it is in-line
200 with other work that questioned whether “pure” object recognition systems really were the best models
201 of ventral stream physiology^{26,27}. To this body of work, we add the observation that semi-supervised
202 algorithms (inspired by the machine learning work of Ref. 20) could be even better than the “pure”
203 unsupervised learning algorithms.

204 Compellingly, and in line with our findings, recent studies of human perceptual judgments of object
205 categories showed that neural networks that combined an image-generative component with a
206 classification component, gave closer matches to the human behavioral data than did networks without
207 the generative component²⁸. In other words, both in terms of human perceptual judgments²⁸, and primate
208 neurophysiology (this work), our best understanding of VS computation might be in terms of a
209 combination of different task objectives, that include object recognition and image reconstruction. I.e.,
210 semi-supervised models might form our best models of the VS.

211 Somewhat surprisingly, we found that categorization performance in our “combined” model was nearly
212 as good as in our “classify” model (Fig. 1D), even though the units in the “combined” model were
213 overall less category-selective than were the units in the “classify” model (Fig. 3D). This apparent
214 contradiction is explained by a recent machine learning study²⁹, which trained neural networks for object
215 categorization, using regularization that penalized category selectivity in all but the readout layer. This
216 led to networks with much lower single-unit category selectivity, but no commensurate loss in
217 categorization performance at the read-out stage. Thus, the link between single-unit category selectivity,
218 and overall network categorization performance, is surprisingly weak.

219 Importantly, our goal here was not necessarily to obtain state-of-the-art models of the primate VS.
220 Rather, it was to compare different objective functions within the same architecture, to see which was a
221 better match to the VS. Some recent work of ours¹⁶ does push more towards obtaining state-of-the-art
222 models, and finds that networks trained end-to-end to predict V1 firing rates achieve higher performance
223 than is obtained using regression against the unit activations from VGG-16 (a pre-trained object
224 classification network). That suggests that there is something more going on in primate VS than “just”
225 object recognition, although another study concurrent to that one¹⁷ found that regression on VGG-16
226 activations was slightly better than end-to-end trained models. For many reasons (different datasets, and
227 different inclusion criteria for neurons, for example), direct comparison of performance measures
228 between those studies is difficult. As such, an important future area of work is to systematically sample
229 the space of architectures and objective functions, to find the best one. Our work suggests that semi-
230 supervised objectives are strong candidates for that work, and we are encouraged by efforts like the
231 Brain-Score platform³⁰, to facilitate quantitative comparison between models.

232 One natural question that arises is about our decision to train our models on images of fashion items
233 superimposed on natural image backgrounds, as opposed to other datasets (e.g., ImageNet). We chose
234 this approach because it yielded images of naturalistic objects (clothing items) with rich natural image

235 backgrounds, yet was parametric in the location and orientation of the objects, and highly tractable
236 computationally. The same is not true of ImageNet or other “typical” computer vision benchmark tasks.
237 Moreover, being able to procedurally generate new examples (of clothing items on nature image
238 backgrounds) during training gave effectively endless variation in the training data that improved the
239 training of our models.

240 Moreover, while we chose canonical correlation analysis (CCA) for comparing neural data to neural
241 network models, many recent studies^{2,4,14-17} (including some of our own^{16,31}) used instead analyses based
242 on representational dissimilarity matrices (RDM), or regression between neural network unit activations
243 and recording neuronal activities. While we like the RDM and regression approaches, all of them
244 (including CCA) have important limitations, leaving it unclear which is the best method to compare
245 neural networks to brains. First, RDM compares matrices of image-by-image (or category-by-category)
246 dissimilarity in activation vectors in the neural network, to those obtained from the brain³². In this
247 approach, even if the neurons in the brain were exactly recapitulated by units in the neural network, the
248 RDM analysis could still show a poor match if there are *other* units in the neural network that do not
249 match those in the brain from which the experimenters recorded. Given that neural data is invariably
250 subsampled (not all neurons are recorded), this can be serious limitation. Regression-based approaches
251 get around this challenge by attempted to reconstruct the neuronal activities from the neural network
252 unit activations. A downside to this approach is the need for heavy regularization to prevent overfitting,
253 and the difficulty in deciding how to average the prediction quality (usually a correlation, or fraction of
254 explained variance) over neurons to get ensemble statistics. Those values are typically just averaged
255 over cells, but neurons’ activations are usually correlated with each other, so that averaging can be
256 problematic. CCA attempts to circumvent these issues, by finding linear combinations of neural network
257 unit activations, that most correlate with linear combinations of neuronal activities. When multiple
258 components are obtained, they are each independent of one another, enabling us to average over their
259 correlation values (we used 10 CCA components in this study). For these reasons and others, an

260 increasing number of neuroscientists are using CCA for analyses like the one presented here^{22,23}. We do
261 not intend here to argue that any one of these methods is better than any other. All of them have
262 limitations, and an important avenue for research is to determine, on principled grounds, which approach
263 is best for different types of comparisons between brains and artificial neural networks.

264 It is important to mention that this study had several important limitations. First, we studied only a
265 single neural network architecture. In principle, different results could be obtained with other
266 architectures. At the same time, the concurrent results from other groups^{14,15} (using other architectures
267 and image datasets), showing that unsupervised learning provides better VS models than does
268 supervised learning, increases our confidence in our findings. Second, our results from images of
269 fashion items on nature scene backgrounds could, in principle, fail to generalize to other settings. On the
270 other hand, natural images have strong statistical regularities^{33,34}, suggesting that, so long as one samples
271 broadly from the realm of realistic images, the specific images chosen may not be overly important. Our
272 images – of real-world objects on nature image backgrounds – should thus not pose any serious issues.

273 We conclude by noting that a key open question in neuroscience is to find the computational objectives
274 that describe the visual ventral stream. Our work suggests that semi-supervised objectives, combining
275 object recognition with scene reconstruction, may be promising candidates.

276

277 Materials and Methods

278 Primate Electrophysiology

279 Neural recordings were originally collected by the DiCarlo lab (Ref. 12) and shared with us for this
280 analysis. In brief, neural recordings were collected from the visual cortex of two awake and behaving
281 rhesus macaques using multi-electrode array electrophysiology recording systems (BlackRock
282 Microsystems). Animals were presented with a series of images showing 64 distinct objects from 8

283 classes rendered at varying position in the animal's visual field, and with variation rotations. After
284 spike-sorting and quality control this resulted in well-isolated single units from both IT (n=168) and V4
285 (n=128); higher-order areas in primate visual cortex. A full description of the data and experimental
286 methods is given by Ref. 12.

287 **Dataset and Augmentation**

288 Our goal was to study the object representations, scene reconstruction, and representation of non-
289 categorical information, within artificial neural networks. To achieve that goal, we trained the neural
290 networks to take in images, and either categorize the objects within them, reconstruct the images, or
291 categorize the objects *and* reconstruct the input (i.e., a semi-supervised autoencoder²⁰). To train these
292 networks, we required images that varied in categorical, and in non-categorical, properties. For that
293 reason, we constructed images of clothing items superimposed at random locations over natural image
294 backgrounds.

295 To achieve this goal, we used all 70,000 images from the Fashion MNIST dataset, a computer vision
296 object recognition dataset comprised of images of clothing articles from 10 different categories. We
297 augmented this dataset by superimposing those 28x28 pixel images onto 112x112 pixel frames, with the
298 center locations drawn randomly from a uniform distribution spanning 75% of the image field. Images
299 were shifted according those randomly drawn dx and dy values, and rotated according to randomly
300 drawn angles between -54 and +54 degrees. After applying positional and rotational shifts, the objects
301 were superimposed over random patches extracted from natural images from the BSDS500 natural
302 image dataset to produce simplified natural scenes which contain categorical (1 of 10 clothing
303 categories) and non-categorical (position and rotation shifts) variation. Random 112x112 pixel patches
304 from the BSDS500 dataset were gray scaled before the shifted object images were added to the
305 background patch (Fig 1A). All augmentation was performed on-line during training. That is, every
306 position shift, rotation shift, and natural image patch was drawn randomly every training batch instead

307 of pre-computing shifts and backgrounds. This allows every training batch to be composed of unique
308 combinations of objects, backgrounds, rotations, and shifts, helping to prevent overfitting. This approach
309 yielded 112x112 pixel images that contained the clothing item, at a random location and orientation,
310 with a nature image background.

311 **Computational models**

312 The convolutional models were constructed by sequentially combining convolutional layers, followed
313 by an all-to-all connected layer (z). Each convolutional layer receives as input a spatially arranged map
314 from the prior layer. A filter kernel is multiplied against the input at each spatial location in the input,
315 and the resultant value is added to the bias and passed through the nonlinear activation function.

316 The models described in our paper were constructed according to the table below. The first 4 layers were
317 convolutional, whereas the latent layer (z) was densely connected.

	<i>Output Size</i>	<i>Kernel</i>	<i>Activation</i>	<i>Dropout</i>	<i>Batch Normalization</i>
					<i>Size</i>
<i>Input</i>	112 x 112	N/A	N/A	N/A	N/A
<i>Layer 1</i>	56x56x16	3x3	LeakyReLU	25%	0.8
<i>Layer 2</i>	28x28x32	3x3	LeakyReLU	25%	0.8
<i>Layer 3</i>	14x14x64	3x3	LeakyReLU	25%	0.8
<i>Layer 4</i>	7x7x128	3x3	LeakyReLU	25%	0.8
<i>Latent, z</i>	500		Linear	0%	0.8

318 Models using the “reconstruct” objective, and the “composite” classify-and-reconstruct objective (see
319 below) need an additional generator network to reconstruct the original stimulus input from the latent
320 representation. The generator network (G) uses a residual convolutional neural network (ResNet) which
321 has achieved state of the art performance in natural image generation. The generator network uses is
322 comprised of deconvolutional layers and its architectural hyperparameters directly mirror those in the
323 convolutional encoder. We chose this generator network structure because it led to better performance
324 (lower sums of squared errors in image reconstruction) than other generators we had tried, including
325 ones that mirrored the encoding side of our network models. We do not claim that this generator model
326 describes anything about the biology: it is there instead to enable an image to be decoded from the latent
327 representation, to help test whether the latent representation contains sufficient information for that
328 reconstruction.

329 Our models can be found on Github (<https://github.com/elijahc/vae>).

330 **Objective functions and training parameters**

331 Models optimized for classification use categorical cross-entropy for the objective function. Categorical
332 cross-entropy (XENT) is a commonly used objective function in machine learning to train neural
333 network classifiers. Multilabel cross-entropy is calculated according to the equation below where M is
334 the total number of classes

$$335 \quad XENT = - \sum_{c=1}^M y_c \cdot \ln(\hat{y}_c)$$

336 Here, y_c is the true category label, represented as a one-hot vector, and \hat{y}_c is the network output
337 obtained from the linear readout of the latent state (see Fig. 1).

338 Models optimized for reconstructing the original input scene use pixel-wise sum of squared error (SSE)
339 between the input and the generator's output (\hat{x}).

340

$$SSE = \sum (x - \hat{x})^2$$

341

342 Models optimized for both objectives (i.e., the “combined” objective) were optimized for the sum of the
343 two: their objective function was $SSE + XENT$.

344 Notably, other objective functions could also have been used for the reconstruction loss, in place of our
345 SSE objective. One example would be the contrastive loss (as in Ref. 14). We do not claim that the SSE
346 is the only (or even the “best”) loss function for the unsupervised learning component. Minimizing this
347 loss does, however, force the network’s latent representation to retain sufficient information about the
348 input to enable its reconstruction.

349 We trained each model in our experiment until classification accuracy plateaued on a validation dataset
350 of 512 objects from the 10,000 test images in the fashion MNIST dataset.

351 **Model Evaluation**

352 Canonical Correlation Analysis (Fig. 2):

353 We quantified the similarity of each models’ layer-wise selectivity to corresponding layers in primate
354 ventral stream using Canonical Correlation Analysis (CCA)²². CCA finds a set of weights used to
355 project both the primate electrophysiology results and our own model unit activations into a lower
356 dimensional space and measures the correlation of the projections in this space. The projection weights
357 are optimized to maximize correlation in the lower dimension. We use 10 projection dimension for this
358 analysis and report the average over the (optimized) correlations of those 10 dimensions. In analogy to
359 the monkey experiments, we performed these analyses on randomly-chosen sets of 250 units from our

360 models; this approximates the number of pseudo-randomly sampled of neurons with the implanted
361 electrode arrays. While these 250 units represent 50% of our latent space (z), the fraction of neurons
362 sampled from monkey V4 or IT in the physiology experiments was much lower.
363 We repeated the analysis for 15 different random draws of unit activations and report the distribution of
364 correlations over those 15 draws (Fig 2).

365 Feature Selectivity (Fig. 3):

366 After training performance plateaus, 5-fold sampling of 250 randomly chosen unit activations from each
367 layer in the encoder model (Fig 1B) were used in comparisons with primate ventral stream
368 electrophysiology. Unit activations were generated using a random sample from held out test images
369 (not used during training). As in a (simulated) electrophysiology experiment, each image was input to
370 the network, and the corresponding unit activations were recorded. We then analyzed these unit
371 activations in the same way as we did the firing rates recorded in monkey visual cortex, described
372 below.

373 First, we measured selectivity of our artificial neurons to different image attributes, in the same way as
374 Ref. 12 (they call these measures “performance” instead of selectivity). For continuous-valued scene
375 attributes (e.g. horizontal position) we measured selectivity as the absolute value of the Pearson
376 correlation between the neuron’s response and that attribute in the stimulus image. For categorical
377 properties (e.g. object class) we measure selectivity as the one-vs-all discriminability (d').

378 Acknowledgements

379 We would like to thank the DiCarlo lab for sharing their primate electrophysiology recordings with us.
380 Special thanks to Alon Poleg-Polsky for thoughtful discussion and direction and to Doug Crawford, Shaiyan
381 Keshvari, Martin Schrimpf, Rachel Sewell, and Heidi Sjoberg for helpful feedback on the manuscript. EC
382 acknowledges funding by an NDSEG fellowship through the US Department of Defense. JZ acknowledges funding
383 from CIFAR, the A.P. Sloan Foundation, Google, the Canada Research Chairs Program, and the Natural Sciences
384 and Engineering Research Council of Canada (NSERC, RGPIN-2019-06379).

385 References

386 1. Felleman, D.J. & Van Essen, D.C. *Cereb. Cortex* **1**, 1–47 (1991).

387 2. Yamins, D.L.K. et al. *Proc. Natl. Acad. Sci. U.S.A.* **111**, 8619–8624 (2014).

388 3. Kriegeskorte, N. et al. *Neuron* **60**: 1126–1141 (2008).

389 4. Khaligh-Razavi, S., and Kriegeskorte, N. *PLoS. Comput. Biol.* **10**: e1003915 (2014).

390 5. Bell, A.H. et al. *J Neurophysiol.* **101**: 688–700 (2009).

391 6. Yamins, D.L.K. & DiCarlo, J.J. *Nat. Neurosci.* **19**, 356–365 (2016).

392 7. Cadieu, C.F. et al. *PLoS Comput. Biol.* **10**, e1003963 (2014).

393 8. Güçlü, U. & van Gerven, M.A.J. *J. Neurosci.* **35**, 10005–10014 (2015).

394 9. Stokes, M., Thompson, R., Cusack, R. & Duncan, J. *J. Neurosci.* **29**, 1565–1572 (2009).

395 10. O'Craven, K.M. & Kanwisher, N. *J Cogn Neurosci* **12**, 1013–1023 (2000).

396 11. Chen, Y. & Crawford, J.D. *Annals of the New York Academy of Sciences* **46**, 774 (2019).

397 12. Hong, H., Yamins, D.L.K., Majaj, N.J. & DiCarlo, J.J. *Nat. Neurosci.* **19**, 613–622 (2016).

398 13. Richards, B.A. et al. *Nat. Neurosci.* **22**, 1761–1770 (2019).

399 14. Konkle, T., and Alvarez, G.A. *biorXiv* 10.1101/2020.06.15.153247 (2020).

400 15. Zhuang et al. *biorXiv* 10.1101/2020.06.16.15556 (2020).

401 16. Kindel, W., Christensen, E., and Zylberberg, J. *J. J. Vision* **19**: 29 (2019).

402 17. Cadena, S.A. et al. *PLoS Comput. Biol.* **15**: e1006897 (2019).

403 18. Zylberberg, J., Murphy, T.M., and DeWeese, M.R. *PLoS Comput. Biol.* **7**: e1002250 (2011).

404 19. Carandini, M. & Heeger, D.J. *Nat. Rev. Neurosci.* **13**, 51–62 (2011).

405 20. Cheung, B., et al. *arXiv*: 1412.6583 (2014).

406 21. Majaj, N.J., Hong, H., Solomon, E.A. & DiCarlo, J.J. *J. Neurosci.* **35**, 13402–13418 (2015).

407 22. Sussillo, D., Churchland, M. M., Kaufman M. T., & Shenoy, K.V. *Nat. Neurosci.* **18**: 1025–1033 (2015).

408 23. Wang, H.T. et al. *NeuroImage* **116**: 745 (2020).

409 24. Olshausen, B.A., and Field., D.J. *Nature* **381**: 607–609 (1996).

411 25. Rehn, M., and Sommer, F.T. *J. Comput. Neurosci.* 22: 135-146 (2007).

412 26. Conway, B. *Ann. Rev. Vis. Sci.* 4: 381-402 (2018).

413 27. Yamins, D. and DiCalro, J. *Curr. Opin. Neurobiol.* 37: 114-120 (2016).

414 28. Golan, T., Raju, P.C., and Kriegeskorte, N. *Proc. Natl. Acad. Sci. USA* 117: 29330-29337
415 (2020)

416 29. Leavitt, M., and Morcos, A. arXiv: 2003.01262 (2020).

417 30. Schrimpf, M., et al. *Neuron* 108: 413-423(2020).

418 31. Federer, C., et al. *Neural Netw.* 131: 103-114 (2020).

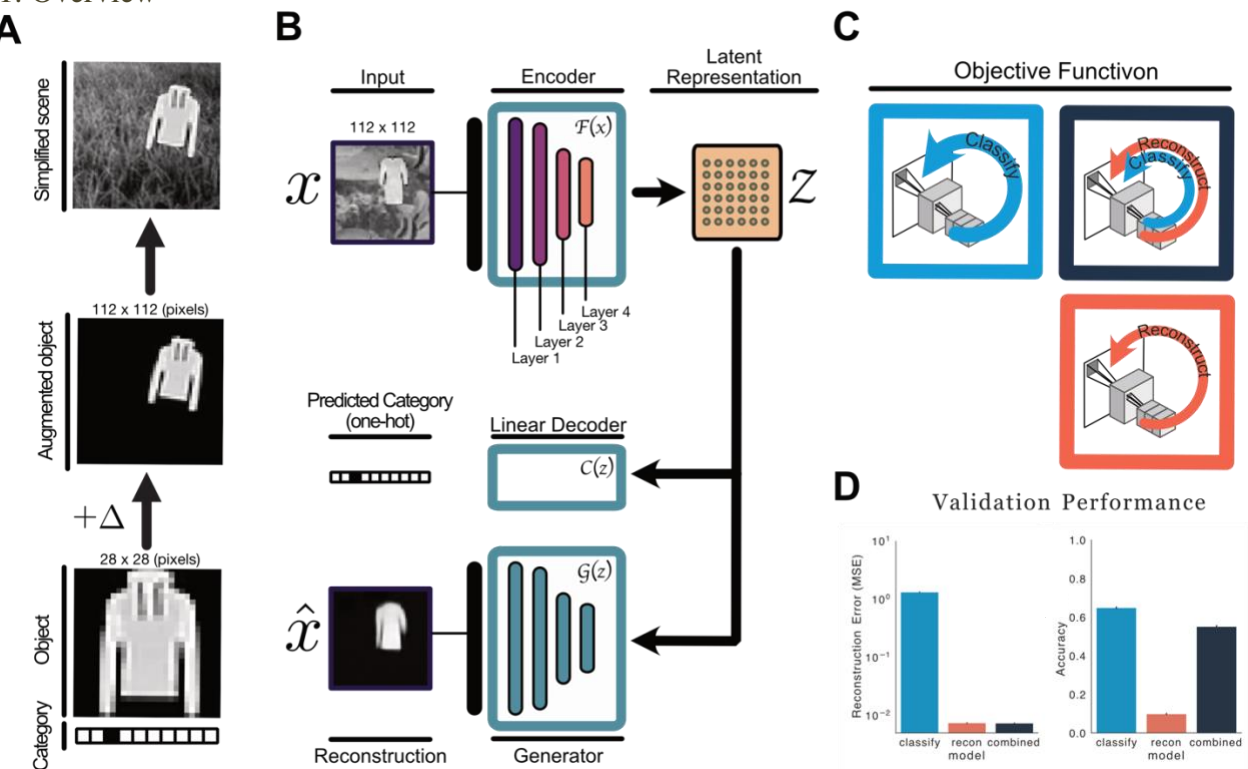
419 32. Kriegeskorte, N., Mur, M., and Bandettini, P. *Front. Syst. Neurosci.* 2: 4 (2008).

420 33. Ruderman, D., and Bialek, W. *Adv. Neural. Info. Proc. Syst.* 6: 551-558 (1993).

421 34. Zylberberg, J., Pfau, D., and DeWeese, M.R. *Phys. Rev. E.* 86: 066112 (2012).

422

Fig. 1: Overview



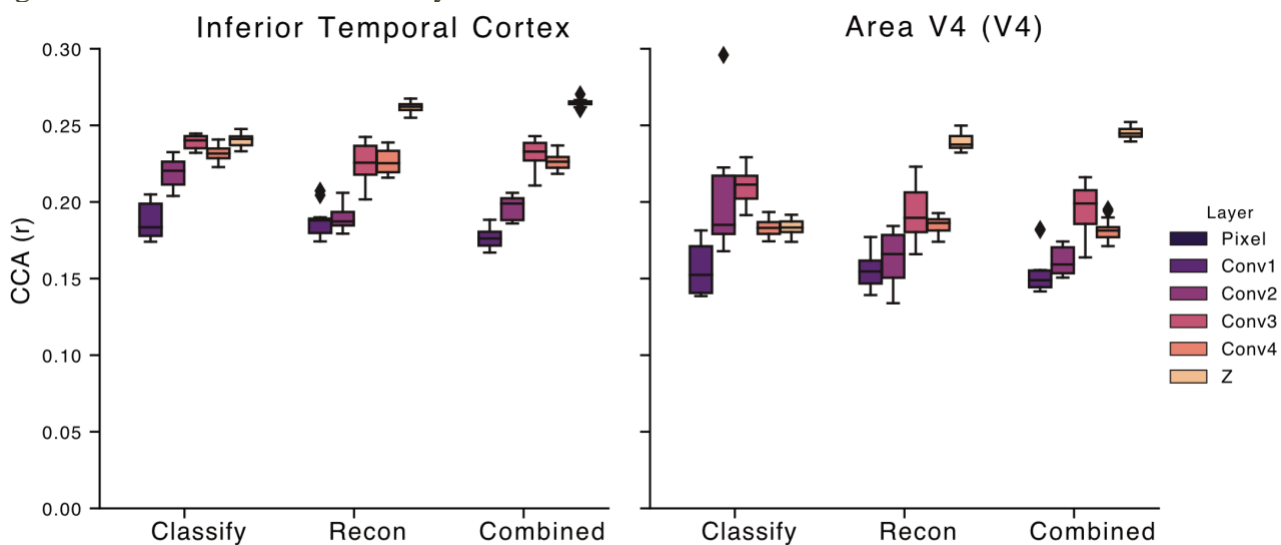
423

424 **A)** We constructed images of clothing items superimposed over natural image backgrounds at random
 425 eccentricities and orientations. **B)** We model the ventral stream as an encoder whose objective is to map
 426 input image (x) onto more abstract “latent” representations (z). In our models this latent space contains
 427 500 artificial neurons. The latent layer (z) is densely connected whereas the preceding layers were all
 428 convolutional (see Methods). The generator network (G) uses these latent representations (z) as input to
 429 reconstruct the object at the correct location within the scene. A separate linear decoder attempts to
 430 determine the object identity from the activities of the units in z . **C)** We trained these neural networks on
 431 one of three tasks: object categorization (“classify”), object reconstruction (“reconstruct”), or object
 432 categorization with concurrent image reconstruction (“combined”). **D)** Object categorization and
 433 reconstruction performance of the three networks after they were trained, assessed on held-out images
 434 (i.e., ones not used in training the networks).

435

436

Fig. 2: Canonical Correlation Analysis



437

438

We used Canonical Correlation Analysis (CCA) to quantify how similar the responses in the layers of each model were to primate electrophysiology data in both inferior temporal cortex (IT) and visual area V4 (V4). We used random draws of 250 unit activations in each layer of the fully trained convolutional models optimized under the “classify” objective (categorical cross-entropy, left in each panel), the image reconstruction objective (“recon”), and the “combined” classify and reconstruct semi-supervised autoencoder objective. For each comparison between a given neural network layer and brain area, we computed the canonical correlations of the first 10 CCA components, and averaged their values. We repeated this process for 15 random draws of the neural network unit activations, and display the distribution of the resultant CCA correlation values (over those 15 draws) as a box and whisker plot. Lines within the filled bar indicate the mean, and filled rectangle corresponds to the interquartile range.

448

449

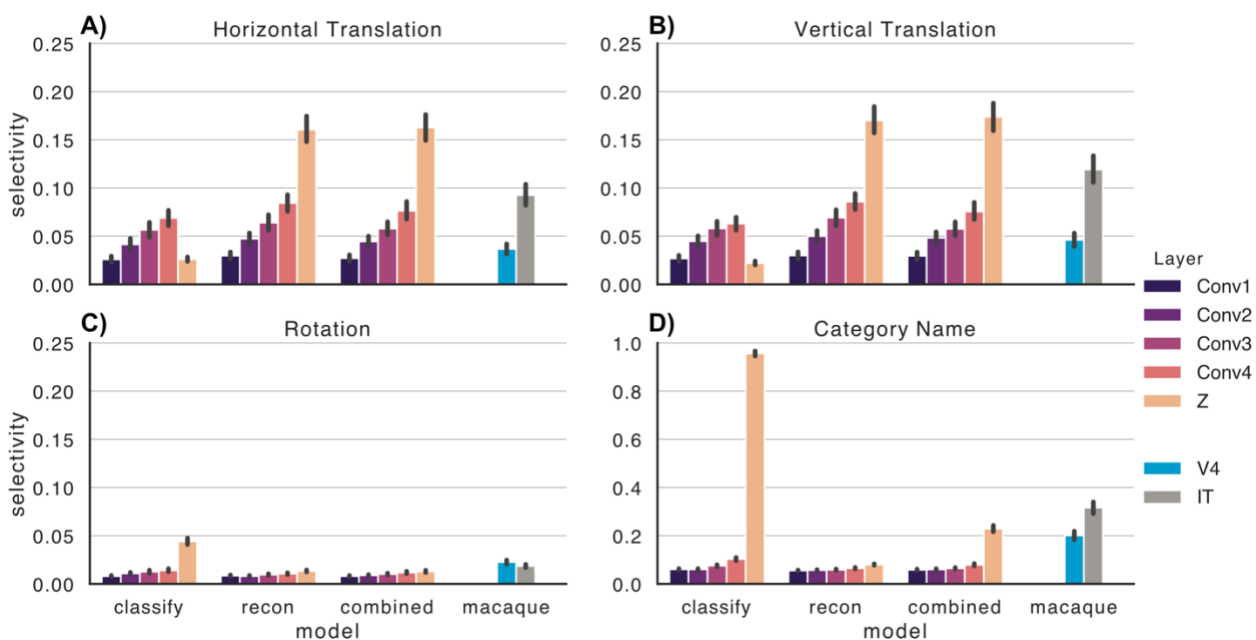
450

451

452

Fig. 3: Selectivity for visual scene attributes

453



454

455

Selectivity of units in the fully trained convolutional models optimized under “classify” objective (categorical cross-entropy), “reconstruction” objective, and the “combined” classify+reconstruct semi-supervised autoencoder objective²⁰. We measured property selectivity of both categorical (**D**) and continuous valued category-orthogonal properties (**A, B, C**) on units in the multi-electrode array data from Hong et al. (2016), and from units in each layer of the computational model encoders. We defined selectivity for categorical information on each unit in the dataset as the absolute value of that unit’s discriminability (one-vs-all d-prime). We defined selectivity for continuous valued attributes (horizontal and vertical position) on each unit as the absolute value of the Pearson correlation coefficient. Unit activities for models were sampled using 10000 held out test images to generate activations at each layer of the model. We randomly sampled 250 units from each layer of each model for the analysis. Error bars show 95% confidence intervals over the observed set of units.